PROCEEDINGS, Thirty-Eighth Workshop on Geothermal Reservoir Engineering
Stanford University, Stanford, California, February 11-13, 2013
SGP-TR-198

MICRO-SEISMICITY WITHIN THE COSO GEOTHERMAL FIELD, CALIFORNIA, FROM 1996-2012

J.O. Kaven[1], S.H. Hickman[1], and N.C. Davatzes[2]

[1]U.S.G.S. Earthquake Science Center
345 Middlefield Rd
Menlo Park, CA, 94025, USA
e-mail: okaven@usgs.gov

[2]Temple University,
1901 N 13th St
Philadelphia, PA, 19122

ABSTRACT

We extend our previous catalog of seismicity within the Coso Geothermal field by adding over two and a half years of additional data to prior results. In total, we locate over 16 years of seismicity spanning from April 1996 to May of 2012 using a refined velocity model, apply it to all events and utilize differential travel times in relocations to improve the accuracy of event locations. The improved locations elucidate major structural features within the reservoir that we interpret to be faults that contribute to heat and fluid flow within the reservoir. Much of the relocated seismicity remains diffuse between these major structural features, suggesting that a large volume of accessible and distributed fracture porosity is maintained within the geothermal reservoir through ongoing brittle failure. We further track changes in b value and seismic moment release within the reservoir as a whole through time. We find that b values decrease significantly during 2009 and 2010, coincident with the occurrence of a greater number of moderate magnitude earthquakes ($3.0 \leq M_L < 4.5$). Analysis of spatial variations in seismic moment release between years reveals that localized seismicity tends to spread from regions of high moment release into regions with previously low moment release, akin to aftershock sequences. These results indicate that the Coso reservoir is comprised of a network of fractures at a variety of spatial scales that evolves dynamically over time, with progressive changes in characteristics of microseismicity and inferred fractures and faults that are only evident from a long period of seismic monitoring analyzed using self-consistent methods.

INTRODUCTION

Geothermal reservoirs derive their capacity for fluid and heat transport in large part from faults and fractures. Micro-seismicity generated on such faults and fractures can be used to identify larger fault structures as well as fractures that provide access to hot rock and the fluid storage and recharge capacity necessary to have a sustainable geothermal resource. The Coso Geothermal Field (CGF), located east of the Sierra Nevada batholith, is situated in a tectonically active region that features strike-slip and normal faults as well as numerous magmatic intrusions evident at the surface as rhyolite domes (Duffield et al., 1980; Manley and Bacon, 2000). Two groups of major faults can be distinguished at the surface based on their orientation and style of faulting (Fig. 1a): north-west trending faults with dextral strike-slip that form prominent lineaments with uncertain ages (Duffield et al., 1980; Unruh and Hauksson, 2006; Davatzes and Hickman, 2006, 2010) and north to north-east trending normal faults that dip both west and east and may have been active in the Quaternary (Hulen, 1978; Unruh and Hauksson, 2006; Davatzes and Hickman, 2006). These faults appear to divide the reservoir into two distinct compartments: the main field and the east flank, (Fig.1) as evidenced by analysis of temperature logs (Kaven et al., 2011) and by clustered microseismicity (Fig. 1b).

Seismicity within the CGF occurs both tectonically and as a consequence of injection and production within the field (Monastero et al. 2005). The seismicity is recorded by the Navy Geothermal Program Office (GPO) using a combination of down-hole and surface seismometers. Initial locations by the GPO generally reveal diffuse clouds of seismicity that occur predominantly in the main field and the

east flank. These "clouds" do not clearly coincide with the mapped fault traces at the surface (Fig. 1). (See also Davatzes and Hickman 2006, 2010 for a more detailed map). Subsurface imaging of fault structure using reflection seismic (Monastero et al., 2005) or magnetotelluric (MT) techniques (Newman et al., 2008) also lacks sufficient resolution to clearly identify discrete structures. Thus, the relationship of these earthquake locations to reservoir-scale fault structure at depth remains poorly constrained.

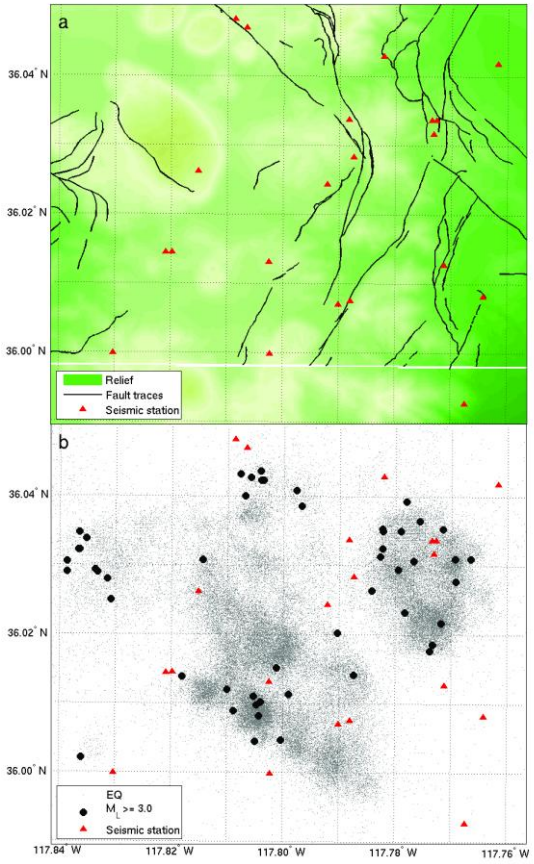

Figure 1: a) Map of the Coso Geothermal Field (CGF) showing topographic relief, mapped surface fault traces (black lines), and seismic station locations (red triangles). b) Seismicity catalog spanning from April 1996 to May 2012. Grey dots indicate earthquake locations for events smaller than M_L 3.0. Black dots indicate events with $M_L \geq 3.0$. The east flank is coincident with the cluster of seismicity in the upper right-hand corner, and the main field corresponds to the more diffuse seismicity to the west and southwest (see field boundaries and well locations in Kaven et al., 2012). Seismic stations are shown as red triangles.

Several studies have used data recorded by the GPO and surrounding Southern California Seismic Network to analyze earthquakes within and adjacent to the CGF, improve hypocentral locations, and invert for the velocity structure of the greater Coso area (e.g. Lees, 1998; Wu and Lees, 1999; Hauksson and Unruh, 2007; Seher et al., 2011). Others have focused on improving hypocentral locations and obtaining moment tensors for microseismicity associated with individual hydraulic fracturing events (Foulger et al. 2008; Julian et al., 2010). In a regional study of subsurface variations in compressional (Vp) and shear (Vs) velocities from July 1993 to June 1995, Wu and Lees (1999) found low Vp /Vs ratios in the main field at geothermal production depths. They suggest this anomaly might represent a hot, fluid-depleted zone. The goal of our investigation is to augment our existing catalog of seismicity and understand the spatial and temporal changes in seismicity to help delineate subsurface structures and fluid compartmentalization within the CGF. We build on results from Kaven et al. (2012) with a more extensive analysis of the GPO network data to improve locations, develop a newly refined velocity structure, and perform error analyses for relative earthquake locations.

DATA & METHODS

We use seismic data recorded by the Navy GPO from April 1996 to May 2012 at 20 permanent and 30 temporarily deployed stations, most of which are three-component seismometers sampling at either 480Hz or 250Hz. The GPO catalog contains >75,000 earthquakes in the greater Coso region during the time period studied. Consistent measures of hypocentral parameters (location and origin time) and a reliable, one-dimensional starting velocity model are paramount in any location or velocity structure procedure (Kissling et al., 1994). Our work flow included the following sequential activities: 1) updating the existing catalog by manually picking P- and S- arrivals for data after October 2009 until May of 2012; 2) deriving an initial field-wide, one-dimensional (1D) velocity model; 3) inverting for single-event hypocentral parameters using this updated 1D velocity model; 4) using differential travel times of both first arrival times and waveform cross-correlations together with hypocentral parameters derived in Step 2 to relocate all events. This last step is in progress at the time of writing and the catalog used consists of a combination of relocated events and single event locations from step 3.

We manually picked P- and S-arrival times on seismic waveforms that were trigger-recorded by the Earthworm system installed by the Navy GPO. We

compared our picks to those identified by Navy GPO staff prior to November 2009 to ensure continuity in arrival times. In total we inspected and analyzed waveform traces for over 25,800 triggered recordings, each of which having roughly 30 recordings from individual stations. We manage to locate over 60% of the triggered events, resulting in roughly the same number of located events per month as are contained per month in the prior Navy GPO picked catalog.

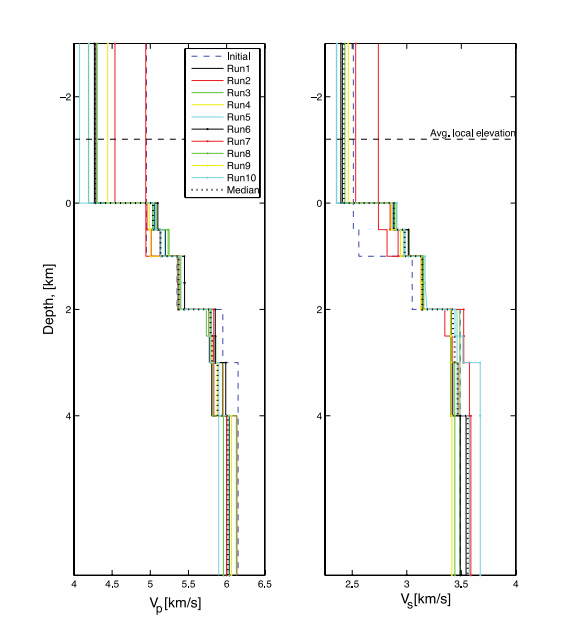

Figure 2: Suite of 1D velocity models derived in this study starting with the initial reference velocity model of Julian et al (2008, dashed blue line). P-wave velocity is on the left and S-wave velocity is on the right. Depths are indicated as km below mean sea level. Separate inversions for 1D velocity structure were obtained using randomly selected events throughout the reservoir. The median solution of the inversions (vertical tick marks) is used in single event locations.

We start by relocating all events using a reference 1D velocity model to ensure that consistent measures of hypocentral parameters form the basis of our relocation and velocity inversion efforts. These relocations were performed with a standard Geiger method inversion starting with the reference 1D velocity model of Julian et al. (2008). Long-lasting catalogs are prone to changes in recording, location routines, and velocity model changes that could introduce undesirable inconsistencies into hypocentral inversions. We find that origin times of events within the CGF, which are critical for relative relocation, vary significantly between the initial Navy GPO catalog origin times and these single event relocations. These differences range from msec to seconds, with an average difference of 60 msec. This demonstrates the importance of performing consistent earthquake relocations throughout the entire Coso catalog, as done in the present study.

Relocation of seismicity and inversion of the seismic velocity structure is a nonlinear problem and thus strongly dependent on the initial 1D velocity structure (Kissling et al., 1994). We compute the1D velocity model solution that minimizes travel time residuals during the simultaneous velocity estimation and event location (Kissling et al., 1994). We carry this procedure out for a suite of randomly selected events within the reservoir to establish a consistent and reliable starting model for our subsequent analyses. We invert for velocities over vertical increments of 0.5 km and thereby attain a finer vertical resolution than used in the reference model (Julian et al., 2008), which has varying resolution but a 1 km vertical resolution for most segments. We use the updated velocity model to then solve for hypocentral parameters (location and origin time) using standard single-event Geiger method inversions and use these solutions for further analyses.

We then use the 1D velocity model to relocate all seismicity using differential travel times from first arrivals and waveform cross-correlated data. The addition of waveform cross-correlated differential travel times permits higher precision differential travel time measurements and aids in refining the structure within the CGF beyond what is possible with the first arrival data (Waldhauser et al., 2004). We apply a causal filter to the waveform data from 5 to 20Hz, the frequency in which most of the energy from these events is contained and across which all seismometers have a constant response. We allow for cross-correlation in 0.5 sec windows around the P-wave arrival and 1 sec around the S-wave arrivals. Differential travel times are used when the correlation coefficient is greater than 0.7, thus ensuring that only very similar waveforms are used. Restricting this analysis to high correlation coefficients also ensures that hypocentral parameters such as location, first motion, and fault attitude, are similar and comparable for correlated events (Waldhauser et al., 2004). The relocation is carried out over geographic tiles that overlap. We utilize these tiles to cut down on memory demand of the inversion code and to ensure that all events are included in the relocation. This process is complete for some portions of the field at the time this report is being written. We report the hypocentral parameters for each event that was relocated in this manner and

use the single event locations where relocation is not yet complete.

We evaluate relative location errors by means of bootstrapping methods in which input data, i.e. differential travel time estimates, are perturbed by 20 msec, or 5 to 6 times the picking accuracy. These are standard statistical methods that perturb the data used in the non-linear location procedure to assess the reliability and accuracy of the results (for detailed discussions on the method see Efron, 1982). The perturbation is based on known and estimated errors in picking recorded by the Navy GPO. We find that relative location errors are comparable throughout the central portion of the CGF (including main field and east flank) and are less than 15 m horizontally and less than 30 m vertically; at the margins of the CGF and away from stations these errors increase.

RESULTS

1D-velocity model

We begin the discussion of our results with the 1D velocity model estimates, since the subsequent analyses (i.e., relocations) strongly depend on consistent and reliable starting velocity models and hypocentral parameters. We start with the initial (reference) model of Julian et al. (2008) and test for model stability by randomly selecting events with M> 0.5 throughout the reservoir to invert for the field-wide 1D velocity model (Vp and Vs) in 10 independent runs (Fig. 2). Although there is considerable scatter in the near-surface velocities (i.e., above mean sea level), our inversions indicate only slightly different velocities than the initial model at greater depths (Fig. 2). For example, the median Vs from our inversions in the shallow portion of the field (i.e., depths of 0 to 2 km below sea level) is higher than the reference model and increases more smoothly with depth. The differences between initial and final (median) models for both Vp and Vs become less significant with greater depth, partly due to fewer events located below 4km, and our median velocities ultimately converge on nearly the same velocities as the reference model.

Event locations

As described above, the full catalog of earthquakes from April 1996 to May 2012 consists of some relocated events and some that have been relocated using the finer 1D velocity model. We use existing Navy GPO phase picks for all years prior to November 2009 and use our phase picks from November 2009 onward, unless Navy GPO picks exist and have smaller single-event location errors when compared to our picks and location results. The hypocenter locations are continuously updated until all events are located. The resultant complete catalog consist of >75,000 events within the CGF (Fig.1b).

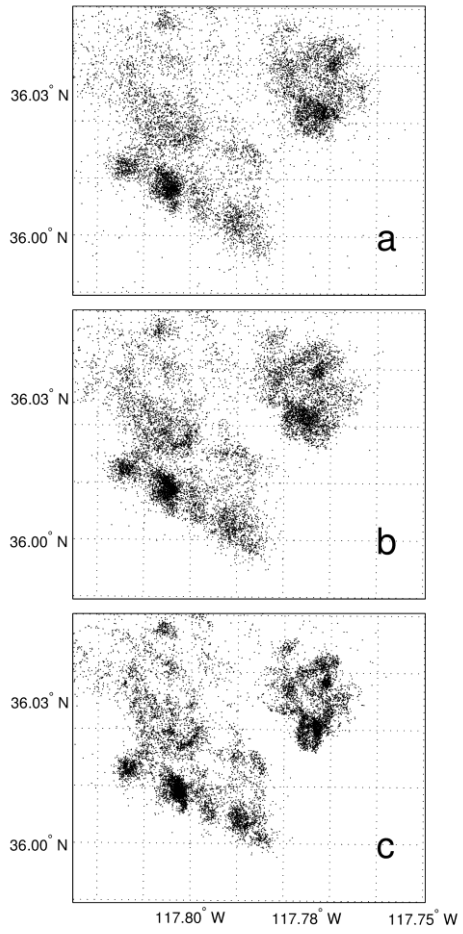

Figure 3: Comparison of event locations throughout the CGF: a) Navy-GPO Catalog; B) Geiger method single event locations using refined 1D-velocity model; c) relative relocations using differential travel times. Only events with $M_L \geq 0.5$ are depicted here. (See Kaven et al 2012 for more detail.)

Seismicity in the CGF is concentrated in the two major compartments, the main field to the southwest and the East Flank to the northeast (Fig. 1b). Nearly all seismicity recorded within the CGF is located within these two compartments, which are separated by a region nearly void of any seismicity through the time period covered by the catalog. This lack of seismicity between the two major compartments likely indicates that both compartments are confined and fluid and heat exchange between the two

compartments may be limited. Further evidence for the separation of the two compartments is provided by temperature data from the CGF, which indicates substantially lower temperatures between these two main compartments than within them (Kaven et al., 2011)

We show results of our differential travel time relocations for the entire field, but restricted to $M_L \geq 0.5$ over the time period April 1996 to March 2008 from Kaven et al. (2012) to highlight the refinement in hypocentral parameters made possible by the relative relocation technique (Fig. 3). Initial locations are significantly more diffuse (Fig.3a) than those located using the refined 1D velocity model with the standard Geiger method (Fig.3b). The full relocation utilizing P- and S-wave differential travel times from picks and waveform cross-correlation significantly sharpens the distribution of earthquakes throughout the reservoir, resulting in more distinct clustering and better definition of through-going structures and compartment boundaries (Fig.3c). Work is now underway to apply these relative relocation techniques to all of the seismic data presented in the present paper, to further define the major structural features and extent of fluid pressure compartmentalization within the Coso reservoir.

DISCUSSION

The full catalog of earthquakes from April 1996 to May 2012 can be used to characterize the temporal and spatial evolution of seismicity within the CGF, even before relative relocations are completed field wide. We calculate b-values from the slope of the magnitude-frequency relationship (Gutenberg-Richter law) using an L1-regression line fit and evaluate the median absolute deviation of our resultant annual b-values. This b-value indicates the relative number of small to large earthquakes for a given area and time period. Here we limit ourselves to the spatial extent of the CGF depicted in Figure 1 and evaluate the b-value for each year separately. The examples shown in Figure 4 for b-value calculations in 2009 and 2010 illustrate the necessary ingredients of a robust b-value calculation. The frequency-magnitude relationship is utilized to find the magnitude of completeness (M_c), below which the decreasing number of events is due to incomplete detection by the local seismic network. The M_c coincides with the "roll-over" in the frequency magnitude curve as the magnitude decreases, which can be successfully determined using the maximum curvature in the frequency-magnitude distribution (Wiemer and Wyss, 2005). Only magnitudes larger than M_c are used in the L1 line fit to calculate the b-value.

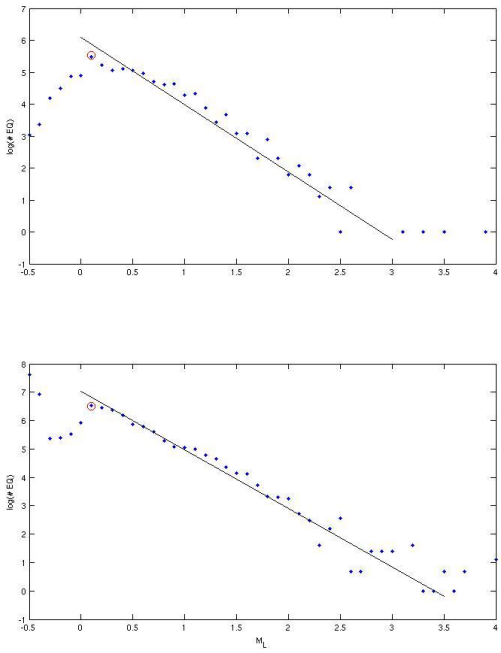

Figure 4: Frequency-magnitude relationship for seismicity within the area outlined in Fig. 1 in 2009 (top panel) and 2010 (bottom panel). Blue dots indicate the magnitude (binned) vs. Log of number of earthquakes. Red circle indicates the magnitude of completeness (M_c, see text); black line is the L1-fit to data with magnitude greater than M_c, the slope of this line is the b-value.

The field-wide b-value ranges from a low in 2009 of 1.75 to a high of 2.4 in 2005, with median absolute deviation remaining fairly uniform at 0.25 throughout the time span covered (Fig. 5a). The drop in b-value in 2001 is the result of a three months' partial outage of the seismic network, which is also reflected in the increased median absolute deviation in 2001 and the increase in M_c (Fig.5b). This partial network outage is also reflected in an increase in the minimum detected event magnitude during the second half of 2001 (Fig. 5c).

The drop in b-value from ~2.2 in 2008 to a minimum of 1.75 in 2009 followed by 1.78 in 2010, however, is not related to instrumentation or processing artifacts and hints at a significant change in the relative occurrence of small to large events. Similar changes in b-value have been observed elsewhere and attributed to aftershock sequences for moderate to large events, in particular in regions exhibiting initially high b-values (McNutt, 2005) such as is the

case here (Fig. 5a). Although such a relationship is difficult to verify until we examine relocated Coso seismicity more closely, it is worth noting that four moderate events with $M_L \geq 3.0$ occurred in 2009, which is slightly more than occurs in the CGF for a typical year. Also, in January 2010 a M_L 4.4 earthquake occurred within the CGF that was preceded and followed by seven moderate events of $M_L \geq 3.0$ in that same year (Fig. 5c). This increase in frequency of moderate magnitude earthquakes also leads to a significantly increased seismic moment release for 2010 (Fig. 5d). We calculate this seismic moment release by employing a regional moment magnitude relationship and sum the seismic moment over a given year (Hanks and Boore, 1984).

We further grid seismic moment release throughout the years and across the reservoir in an effort to understand the spatial evolution of seismicity across the CGF (Fig. 6). We parse the reservoir into 250m by 250m grid cells and compute the seismic moment release for each grid cell per year using the local moment-magnitude relation. We observe that high seismic moment release rate is localized in the main field compartment in the early years of our catalog, 1996-2001, with relatively little seismic moment release in the east flank of the CGF (c.f., Figs 1b and 6). The seismic moment release rate clearly marks the southwestern compartment boundary for the main field in all years. Starting in 2003, seismic moment release increases in the east flank and the corresponding region of seismicity tends to broaden in spatial extent. The boundaries of the east flank compartment are clearly defined and relatively stationary over time along its eastern and southwestern margins but change through time to the north. Regions of less pronounced temporal change in seismic moment release rate coincide with smaller magnitude seismicity that tends to be more diffuse (c.f. Figs. 1b, 3, 6). In 2010, unusually high seismic moment release is observed in the east flank and a new area of high moment release rate appears to the northwest of the main field, with the sequence of seven events with $M \geq 3.0$ commented on previously contributing significantly to regions of high seismic release rate.

The sharp boundaries defined by the seismic moment release rate probably identify large structural features, e.g. faults, that act as barriers to flow of heat and fluids and thus insulate regions past the boundaries from significant effective stress changes that would otherwise promote seismicity. We will complete relative earthquake relocations throughout the time period covered by this expanded catalog, to more precisely track the migration of seismicity over time and better identify the extent and attitude of these apparent compartment boundaries. Further, we plan to increase our temporal resolution and focus on subsets of the data shown in Figure 6 to investigate whether short-duration changes in injection and production alter the occurrence and locations of regions exhibiting anomalous seismic moment release rate. More clearly identifying the structural boundaries within the CGF, both from event relocations and gridded seismic moment release rates, will aid in our understanding of the loading history of the reservoir as it responds to changes in geothermal production and injection over time.

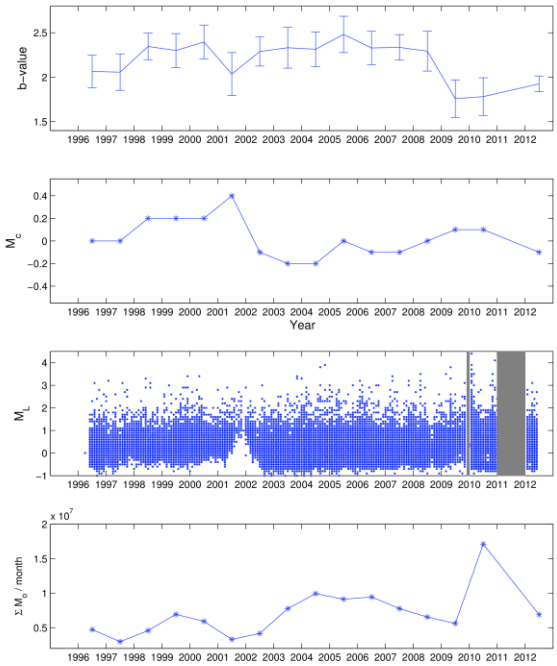

Figure 5: Seismicity characteristics through time within the area outlined in Fig. 1 (tick marks indicate beginning of each year, annual averages are centered on middle of year); a) annual b-value, where error bars indicate median absolute deviation of b-value; b) magnitude of completeness per year; c) event magnitude (M_L), with events binned in increments of 0.1 M_L and 1 month and gray boxes indicate time periods of missing or unverified magnitude calculations. d) Annual seismic moment release rate, normalized by months recorded per year. Note that no robust magnitudes exist yet for 2010 and calculations of b-values, M_c and cumulative moment release are omitted.

CONCLUSIONS

We extended and improved the existing catalog of earthquake locations in the Coso Geothermal Field to cover the time period from April 1996 to May 2012. This involved using Navy GPO picks from April 2008 through October 2009 and hand picking phase arrivals from events field-wide for the period November 2009 to May 2012. We then located all events from 1996 to 2012 using a higher resolution, consistent 1-D velocity model. We continue improving these event locations by relocating events using differential travel times and add to our existing catalog when these relative relocations are completed.

When compared to earlier catalogs from April 1996 through March 2008, this refined catalog and derived spatial variations in moment release rate better define major structural boundaries within the CGF and the locations and temporal evolution of major reservoir compartments. Seismicity and moment release rate in the CGF tend to initiate in very localized regions and then expand from these localized region over time, indicative of aftershock-like sequences. Seismicity characteristics, i.e. b-values and seismic moment release rate, change through time within the CGF as a whole. These changes are most prominent in 2009 and 2010, possible resulting from aftershock sequences following moderate magnitude earthquakes that occurred during these same time periods.

ACKNOWLEDGEMENTS

We thank the Navy GPO and Terra-Gen for permission to use their seismic data. This work was funded by the *DOE Geothermal Technologies Program* under Interagency Agreement DE-EE0001501, with additional support provided by the USGS Energy Resources and Earthquake Hazards Programs.

REFERENCES

Chatterjee, S.N., Pitt, A.M., and Iyer, H.M. (1985), "Vp/Vs ratios in the Yellowstone National Park Region, Wyoming" *Journal of Volcanology and Geothermal Research*, 26, 213-230.

Davatzes, N. C. and Hickman, S. H., (2006), "Stress and faulting in the Coso geothermal field: update and recent results from the East Flank and Coso Wash" *Proceedings 31st Workshop on geothermal Reservoir Engineering, Stanford University, Stanford, California, January 30 – February 1. 2006,* SGP-TR-179, 12p.

Davatzes, N.C. and Hickman, S.H. (2010), "The feedback between Stress, Faulting, and Fluid Flow: Lessons from the Coso Geothermal Field, CA, USA", *Proceedings World Geothermal Congress*, 15p.

Duffield, W. A., Bacon, C. R., and Dalrymple, G. B. (1980), "Late Cenozoic volcanism, geochronology and structure of the Coso Range, Inyo County, California" *Journal of Geophysical Research*, 85, 2381-2404.

Evans, J.R., Eberhart-Phillips, D. and Thurber, C.H. (1994), "User's manual for SIMULPS12 for imaging Vp and Vp/Vs: a derivative of the "Thurber" tomographic inversion SIMUL3 for local earthquakes and explosions" *U.S.Geological Survey, Open File Report*, 94-431, 100pp.

Foulger, G.R., Julian, B.R. and Monastero, F. C. (2008), "Seismic monitoring of EGS tests at the Coso Geothermal area, California, using accurate MEQ locations and full moment tensors" *Proceedings 33rd Workshop on geothermal Reservoir Engineering, Stanford University, Stanford, California, January 28 – 30, 2008,* SGP-TR-179, 8p.

Hanks, T.C. and Boore, D.M. (1984), "Moment-Magnitude relations in Theory and Practice"

Journal of Geophysical Research, 89, B7, 6229-6235.

Hauksson, E. and Unruh, J. (2007), "Regional tectonics of the Coso geothermal area along the intracontinental plate boundary in central eastern California: Three-dimensional Vp and Vp/Vs models, spatio-temporal seismicity patterns, and seismogenic deformation" *Journal of Geophysical Research*, 112, B06309.

Hulen, J. B. (1978), "Geology and alteration of the Coso geothermal area, Inyo County, California" *U.S. Dept. of Energy: Geothermal Energy*.

Julian, B.R., Foulger, G.R. and Monastero, F. C. (2008), "Time-dependent seismic tomography and its application to the Coso Geothermal Area, 1996-2006" *Proceedings 33rd Workshop on geothermal Reservoir Engineering, Stanford University, Stanford, California, January 28 – 30, 2008,* SGP-TR-185, 4p.

Julian, B.R., G.R. Foulger, F.C. Monastero and S. Bjornstad (2010), "Imaging Hydraulic Fractures in a Geothermal Reservoir", *Geophys. Res. Lett., 37*, L07305, 10.1029/2009GL040933

Kaven, J.O., Hickman, S.H. and Davatzes, N.C. (2011), "Micro-Seismicity, Fault Structure and Hydraulic Compartmentilization within the Coso Geothermal Field, California", *Proceedings 36th Workshop on geothermal Reservoir Engineering, Stanford University, Stanford, California, January 31 – February 2, 2011,* SGP-TR-191, 8p.

Kaven, J.O., Hickman, S.H. and Davatzes, N.C. (2012), "Mapping of Fluid Compartments with Micro-Seismicity and Seismic Velocities Within the Coso Geothermal Field, California", *Proceedings 37th Workshop on geothermal Reservoir Engineering, Stanford University, Stanford, California, January 30 – February 1, 2012,* SGP-TR-194, 8p.

Kissling, E., Ellsworth, W.L., Eberhart-Phillips, D. and Kradolfer, U. (1994), "Initial reference models in local earthquake tomography", *Journal of Geophysical Research*, 99, no. B10, 19635-19646

Lees, J. M. (1998), "Multiplet Analyses at Coso Geothermal" *Bulletin of the Seism. Soc. America*, 88, no.5, 1127-1143.

Manley, C.R., and Bacon, C.R., (2000), "Rhyolite thermobarometry and the shallowing of the magma reservoir, Coso volcanic field, California: *Journal of Petrology*, v. 41, p. 149-174.

McNutt, S.R., (2005), "Volcanic Seismology": *Annu. Rev. Earth Planet. Sci.*, v. 33, p. 461-491.

Monastero, F.C., Katzenstein, A.M., Miller, S.J., Unruh, J.R., Adams, M.C. and Richards-Dinger, K. (2005), "The Coso geothermal field: A nascent metamorphic core complex. *GSA Bull.*", **177**(11/12), 1534-1553.

O'Connell, R.J., and Budiansky, B. (1974), "Seismic velocities in dry and saturated cracked solids" *Journal of Geophysical Research*, 79, no. 35 5412-5426.

Schaff, D.P., Bokelmann, G.H.R., Beroza, G.C., Waldhauser, F., and Ellsworth, W.L. (2002)

"High resolution image of the Calaveras Fault seismicity" *Journal of Geophysical Research*, 107, no.B9, 2186, doi 10.1029/2001JB000633.

Schaff, D.P., Bokelmann, G.H.R., Ellsworth, W.L., Zanzerkia, E., Waldhauser, F., and Beroza, G.C. (2004), "Optimizing correlation techniques for improved earthquake location" *Bulletin of the Seism. Soc. America*, 94, no.2, 705-7021.

Seher, T., Zhang, H. Fehler, M., Yu, H., Soukhovitskaya, V., Commer, M. and Newman, G. (2011), "Temporal Velocity Variation beneath the Coso Geothermal Field Observed using Seismic Double Difference Tomography of Compressional and Shear Wave Arrival Times", *GRC Transactions*, v. 90, p. 1743-1747.

Unruh, J. and Hauksson, E. (2006), "Active faulting in the Coso Geothermal Field, eastern California", *GRC Transactions*, v. 30, p. 165-170.

Waldhauser, F. and Ellsworth, W.L. (2000), "A double-difference earthquake location algorithm: method and application to the northern Hayward Fault, California", *Bulletin of the Seism. Soc. America*, 90, 1353-1368.

Waldhauser, F., Ellsworth, W.L., Schaff, D.P. and Cole, A. (2004), "Streaks, mulitplets, and holes: High-resolution spatio-temporal bahavior of Parkfield seismicity", *Geophysical Research Letters*, 31, doi:10.1029/2004GL020648.

Wiemer, S. and Wyss, M. (2005), "Assessing the Quality of Earthquake Catalogues: Estimating the Magnitude of Completeness and its Uncertainty", *Bulletin of the Seism. Soc. America*, 95, 684-698.

Wu, E. and Lees, J. M. (1999), "Three-dimensional P and S wave velocity structures of the Coso Geothermal Area, California, from microseismic travel time" *Journal of Geophysical Research*, 104, no. B6, 13217-13233.

Zhang, H. and Thurber, C.H. (2003), "Double-Difference tomography: the method and its application to the Hayward Fault, California", *Bulletin of the Seism. Soc. America*, 93, no.5, 1875-1889.

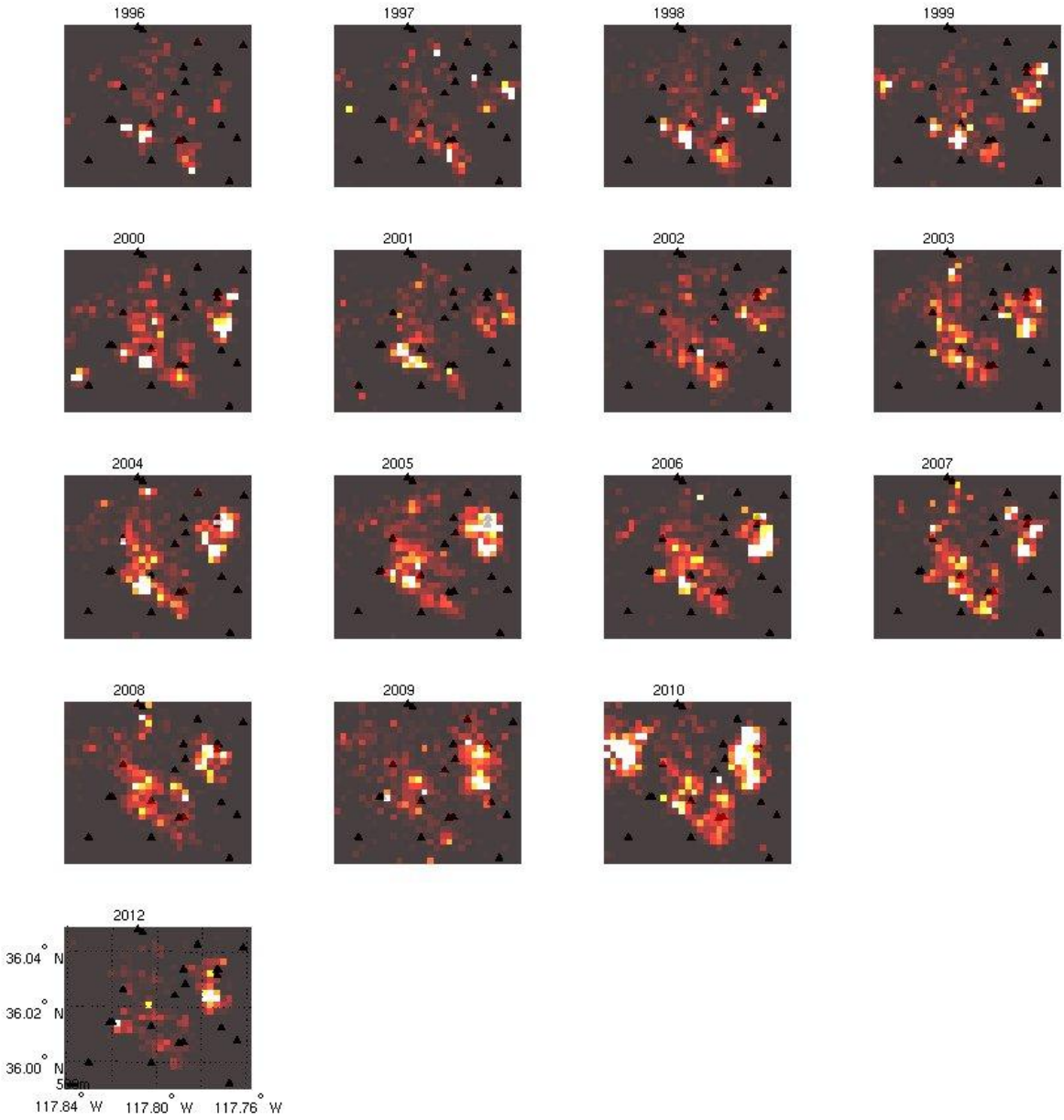

Figure 6: Binned seismic moment release rate for the years shown, where bright colors indicate high moment release rate. Bin edge lengths are 250m. The color scale is normalized to the maximum moment release rate recorded for the years shown. Black triangles depict seismic stations. Note the extent of the area shown is identical to that shown in Fig.1. calculations of b-values, M_c and cumulative moment release are omitted.